



Heterogeneous & Homogeneous & Bio- & Nano-

CHEM **CAT** CHEM

CATALYSIS

Accepted Article

Title: Production of α -ketoisocaproate and α -keto- β -methylvalerate by engineered L-amino acid deaminase

Authors: Yuxiang Yuan, Wei Song, Jia Liu, Xiulai Chen, Qiuling Luo, and Liming Liu

This manuscript has been accepted after peer review and appears as an Accepted Article online prior to editing, proofing, and formal publication of the final Version of Record (VoR). This work is currently citable by using the Digital Object Identifier (DOI) given below. The VoR will be published online in Early View as soon as possible and may be different to this Accepted Article as a result of editing. Readers should obtain the VoR from the journal website shown below when it is published to ensure accuracy of information. The authors are responsible for the content of this Accepted Article.

To be cited as: *ChemCatChem* 10.1002/cctc.201900259

Link to VoR: <http://dx.doi.org/10.1002/cctc.201900259>

WILEY-VCH

www.chemcatchem.org



FULL PAPER

Production of α -ketoisocaproate and α -keto- β -methylvalerate by engineered L-amino acid deaminaseYuxiang Yuan,^[a,b] Wei Song,^[a,b] Jia Liu,^[a,b] Xiulai Chen,^[a,b] Qiuling Luo,^[a,b] and Liming Liu^{*[a,b]}

Abstract: This study aimed to develop an efficient enzymatic strategy for industrial production of α -ketoisocaproate (α -KIC) and α -keto- β -methylvalerate (α -KMV) from L-leucine and L-isoleucine, respectively. L-amino acid deaminase from *Proteus mirabilis* (PmLAAD) was heterologously expressed in *E. coli* BL21(DE3) and modified to increase its catalytic efficiency by engineering the PmLAAD substrate-binding cavity and entrance tunnel. Four essential residues (Q92, M440, T436, and W438) were identified from structural analysis and molecular dynamics simulations. Residue Q92 was mutated to alanine, and the volume of the binding cavity, enzyme activity, and the k_{cat}/K_m value of mutant PmLAAD^{Q92A} increased to 994.2 Å³, 191.36 U mg⁻¹, and 1.23 mM⁻¹ min⁻¹, respectively; consequently, the titer and conversion rate of α -KIC from L-leucine were 107.1 g L⁻¹ and 98.1%, respectively. For mutant PmLAAD^{T436W438A}, the entrance tunnel, enzyme activity, and the k_{cat}/K_m value increased to 1.71 Å, 170.12 U mg⁻¹, and 0.70 mM⁻¹ min⁻¹, respectively; consequently, the titer and conversion rate of α -KMV from L-isoleucine were 98.9 g L⁻¹ and 99.7%, respectively. Therefore, augmentation of the substrate-binding cavity and entrance tunnel of PmLAAD can facilitate efficient industrial synthesis of α -KIC and α -KMV.

Introduction

α -keto acids, organic acids containing a carboxyl group and a carbonyl group, are widely applied in foods, feeds, pharmaceuticals, and chemical synthesis.^[1] A prominent example being compound α -keto acid tablets, a drug containing four α -keto acids, viz., α -ketoisocaproate (α -KIC), α -keto- β -methylvalerate (α -KMV), α -ketoisovalerate (α -KIV), and phenylpyruvate (PPA), as the primary components, which potentially reduces the accumulation of nitrogen waste in patients.^[1b] α -keto acids are synthesized through three different methods, such as (1) chemical synthesis: in the past few decades, the hydantoin process has become one of the primary methods for the preparation of a large amount of α -keto acids, wherein hydantoin is made to react with carbonyl-containing compounds (such as isobutyraldehyde, benzaldehyde, etc.) to generate corresponding hydantoin intermediates,^[2] followed by hydrolysis and acidification

to their respective α -keto acids.^[3] For example, PPA can be synthesized through hydrolysis and acidification of benzylidene hydantoin, an intermediate derived from the reaction between hydantoin and benzaldehyde.^[4] However, owing to the high cost of precursors, multistep chemical reaction, harsh conditions, and production of toxic intermediate,^[5] researchers adopted the (2) fermentation process: α -keto acids can be produced through microbial fermentation, e.g., *Corynebacterium glutamicum* has been used to synthesize α -KIC^[6] and PPA.^[7] Although microbial fermentation is associated with lesser environmental pollution than chemical synthesis, it requires a long duration of fermentation with low productivity.^[6] To further decrease the production cost of α -keto acids, the (3) biocatalytic method with amino acids as the starting material was developed.^[1b]

Biocatalytic technologies to synthesize α -keto acids have been developed in recent years, using amino acid oxidase (AAO, EC 1.4.3.3),^[8] amino acid dehydrogenase (ADH, EC 1.4.1.5),^[9] aminotransferase (AT, EC 2.1.1.X),^[10] and L-amino acid deaminase (L-AAD, EC 1.4.3.2).^[1b] AAO is a flavoenzyme catalyzing the stereospecific oxidative deamination of amino acids to α -keto acids and produces ammonia and hydrogen peroxide. For example, PPA production through D-phenylalanine oxidation by AAO from the porcine kidney has been reported,^[11] with similar results achieved through catalysis of D-methionine to α -keto- γ -methylthiobutyric acid (α -KMTB) by AAO from *Trigonopsis variabilis* CBS 409.^[12] Furthermore, recent studies have focused on recombinant strains expressing enzymes such as ADH.^[13] In the case of ADH, a coenzyme recycling system is required owing to the dependence on the either NADH or NADPH to yield reducing equivalents; hence, such reactions are not cost-effective.^[14] A recent study used L-phenylalanine dehydrogenase derived from *Rhodococcus* sp. M4 to synthesize PPA.^[15] AT catalyzes the reversible oxidative deamination of amino acids to α -keto acids and ammonia, the reverse reaction involving the asymmetric transfer of amino groups to keto acids.^[10] In this process, other keto acids as essential amino acceptors are necessary; however, because of the low reaction equilibrium constant of AT, the reversibility of the AT-catalyzed reactions often decreases the conversion rates.^[10] For instance, *E. coli* tyrosine aminotransferase (EC 2.6.1.5) was previously used to synthesize α -ketoglutaric acid (α -KG) from L-glutamate with a yield of only approximately 50%.^[16] Owing to these limitations, these three enzymes are not suitable for industrial production of α -keto acids. Hence, numerous studies have focused on enzyme L-AAD, a flavin adenine dinucleotide (FAD)-dependent amino acid oxidase, which catalyzes the oxidative deamination of several L-amino acids to the corresponding α -keto acid.^[17] Owing to the numerous advantages of L-AAD, such as non-requirement of an extra cofactor, amino acceptor, and non-production of hydrogen peroxide,^[17] it has been used extensively in synthesizing various α -keto acids, such as PPA,^[18] α -KIV,^[19] α -KG,^[20] α -KMTB,^[21] and α -KIC.^[22] To further increase the titer and

[a] Y. Yuan, W. Song, J. Liu, X. Chen, Q. Luo, Prof. L. Liu
State Key Laboratory of Food Science and Technology
Jiangnan University
Wuxi 214122, China
E-mail: mingll@jiangnan.edu.cn

[b] Y. Yuan, W. Song, J. Liu, X. Chen, Q. Luo, Prof. L. Liu
Key Laboratory of Industrial Biotechnology, Ministry of Education
Jiangnan University
Wuxi 214122, China

Supporting information for this article is given via a link at the end of the document

FULL PAPER

conversion rate of α -keto acids, L-AAD activity was increased through protein engineering strategies,^[18, 21, 23] e.g., L-AAD from *Proteus myxofaciens* was modified through site-directed saturation mutagenesis to increase enzymatic efficiency; consequently, the synthesis rate of α -KIV by the double-mutant strain increased from 2.01 g L⁻¹ to 8.19 g L⁻¹.^[19]

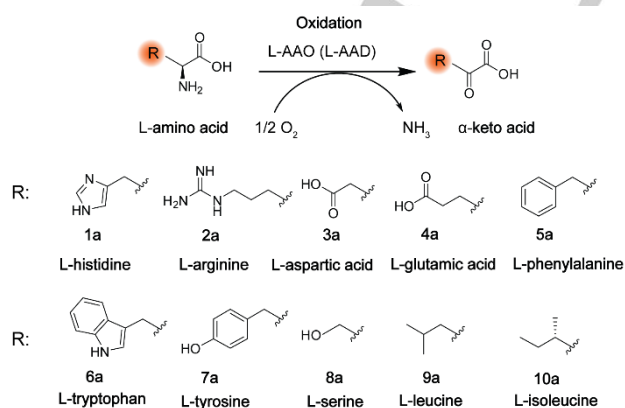
In the present study, a type- I L-AAD (PmLAAD) from *Proteus mirabilis* was selected owing to its broad substrate specificity and heterologously expressed in *E. coli* BL21(DE3). The PmLAAD substrate-binding cavity and entrance tunnel were then engineered for to improve catalytic activity toward L-leucine and L-isoleucine at high substrate concentrations, via site-directed mutagenesis based on the rational design. Finally, the PmLAAD mutants were used to synthesize α -KIC and α -KMV, using a 3-L scale fermenter.

Results

Production of α -KIC and α -KMV via heterologous expression of PmLAAD from *Proteus mirabilis*

As shown in Scheme 1, the amino group of L-amino acids were oxidized to a carbonyl group; consequently, L-amino acids were converted to their corresponding α -keto acids. According to the KEGG database (<https://www.genome.jp/kegg/>), this reaction can be catalyzed by L-AAD, which is extensively present in prokaryotes and eukaryotes.^[9] The characteristics of L-AAD from different microorganisms are enlisted and compared in Supplementary Tables 1 and 2, type- I L-AADs from *Proteus mirabilis* (*P. mirabilis*) exhibited broad substrate specificity toward aliphatic and aromatic-amino acids, typically hydrophobic amino acids. Furthermore, type- I L-AADs encoding *aad* from *P. mirabilis* was cloned and overexpressed in *E. coli* BL21(DE3), and the recombinant strain *E. coli* BL21 (pET28a (+)-PmLAAD) was obtained.

The transformation efficiency of *E. coli* BL21 (pET28a (+)-PmLAAD) was evaluated for ten different L-amino acids (Scheme 1 and Figure 1). *E. coli* BL21 (pET28a (+)-PmLAAD) could not



Scheme 1. L-amino acid deaminase catalyzing the deamination of L-amino acids to α -keto acids.

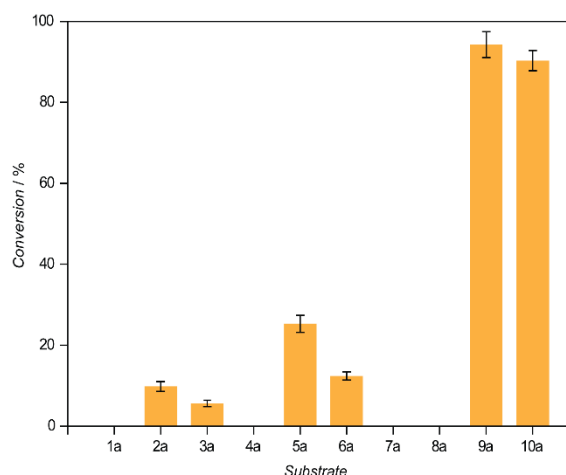


Figure 1. The conversion of PmLAAD^{WT} toward the substrate spectrum.

convert **1a**, **4a**, **7a**, and **8a** to their corresponding keto-acids. For amino acids **2a** and **3a**, the conversion rate was less than $\leq 10\%$. For aromatic amino acids **5a** and **6a**, the conversion rate increased to 10%–30%; however, the conversion rate was increased to $\geq 90\%$ for hydrophobic aliphatic amino acids **9a** and **10a**. These results indicate that *E. coli* BL21 (pET28a (+)-PmLAAD) could efficiently convert L-leucine and L-isoleucine to their corresponding keto-acids α -KIC and α -KMV.

The effect of *E. coli* BL21 (pET28a (+)-PmLAAD) concentration (5–30 g L⁻¹, wet cell weight) on α -KIC production was investigated with 65 g L⁻¹ L-leucine as substrate (Figure 2a), and the α -KIC titer peaked at 62.9 g L⁻¹ with 20 g L⁻¹ wet intact cells, with a 97.5% conversion rate. Furthermore, with 20 g L⁻¹ wet intact cells as catalysts, the conversion rate decreased from 97.5% to 57.3%, and the L-leucine content increased from 65 g L⁻¹ to 110 g L⁻¹ (Figure 2b), as only 62.6 g L⁻¹ α -KIC was produced. Similarly, with L-isoleucine as the substrate to convert to α -KMV by *E. coli* BL21 (pET28a (+)-PmLAAD), 49.4 g L⁻¹ of α -KMV was obtained from 55 g L⁻¹ L-isoleucine and 20 g L⁻¹ wet intact cells, the conversion rate approaching 90.5% (Figure 2c) and then decreasing with an increase in L-isoleucine content (55 to 75 g L⁻¹). consequently, the α -KMV titer remained at approximately 49.4 g L⁻¹ (Figure 2c). These results indicate that the catalytic efficiency of *E. coli* BL21 (pET28a (+)-PmLAAD) is a bottleneck for further increasing the α -KIC or α -KMV titers.

Engineering the substrate-binding cavity and entrance tunnel of PmLAAD

To increase the catalytic efficiency of *E. coli* BL21 (pET28a (+)-PmLAAD), the crystal structure of L-AAD from *Proteus myxofaciens* (PDB entry: 5fjm, 93.74% identity) was selected as a template through a PDB BLAST search, and a theoretical structure of PmLAAD was constructed using SWISS-MODEL. A DALI analysis indicated that the overall structural features of PmLAAD were highly consistent with those of L-AAD from the template (DALI Z-score of 69.9), with a root mean square deviation of 0.1 Å (426 to 426 C α atoms). As illustrated in

FULL PAPER

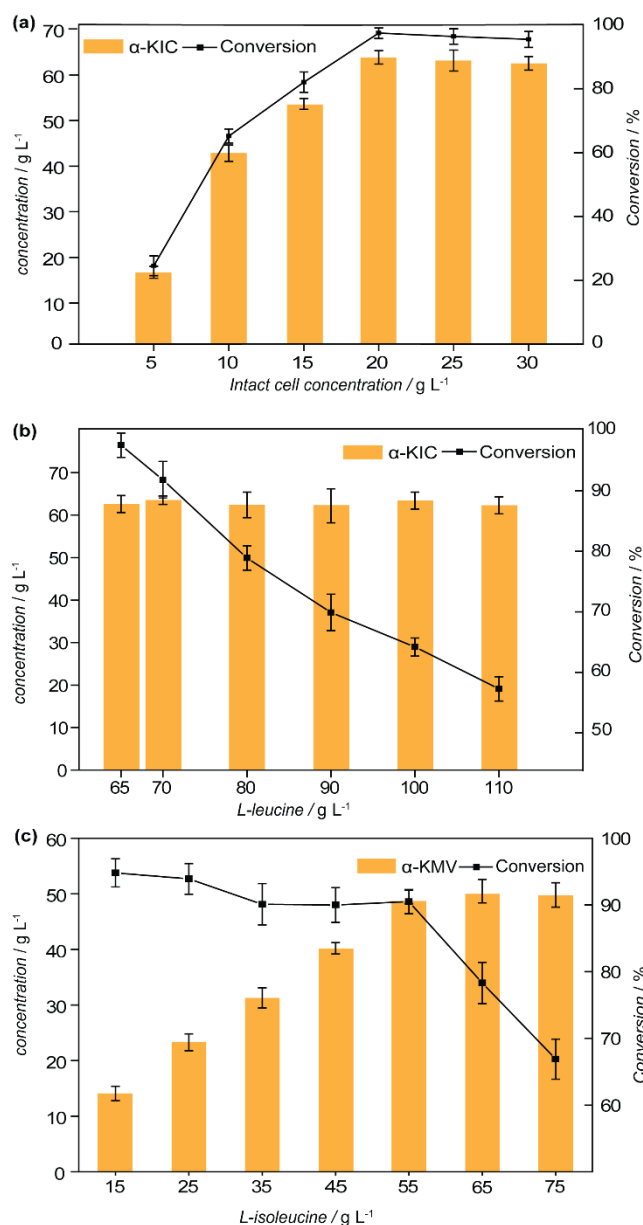


Figure 2. (a) Different concentration of intact cells for α -KIC production; (b) Effect of different L-leucine concentrations on α -KIC production by PmLAAD^{WT}; (c) Effect of different L-isoleucine concentrations on α -KMV production by PmLAAD^{WT}.

Supplementary Figure 1, the PmLAAD model comprises a core domain (with the α + β additional subdomain) and a V-shaped cap domain.

To determine the key residues of the substrate-binding cavity, L-leucine as a substrate and FAD as an important cofactor were docked into the active site of PmLAAD. As illustrated by the binding mode (Figure 3a), L-leucine binds directly at the binding cavity with relatively appropriate positioning and the side chain of Q92 partially occupied the binding sites of L-leucine isopropyl moiety, thus causing steric hindrance, which blocks substrate

binding at the active site, and the other residue M440, which was located proximal to the substrate-binding pocket, toward the carboxyl group of the substrate, potentially results in steric clash between its side chain and FAD. In addition, the backbone of L-leucine is stacked with the FAD isoalloxazine ring, at approximately 3 Å distance (Figure 3a), thus preventing stable L-leucine binding. Therefore, we speculated that Q92 and M440 are key residues affecting the activity of PmLAAD, and hence residues Q92 and M440 were selected for alanine mutagenesis to alter the substrate binding cavity, thereby decreasing the spatial barrier and the steric clash during substrate binding.

As shown by the PmLAAD-L-leucine complex structure, the broad entrance of the active site enables binding with large hydrophobic substrates, whereas the substrate-binding pocket is deep (over 20 Å), and a narrow cavity enclosing the active center displays steric hindrance during substrate entry (Figure 3b). Hence, we speculated a substrate entrance tunnel in the narrow cavity, which potentially regulated substrate entry into the active site, thereby affecting enzyme activity. We then focused on the composition of the entrance tunnel to the active site. CAVER 3.01 was used to identify tunnels present in PmLAAD. As shown in Figure 3c, an 18.88 Å substrate tunnel distance existed in the narrow cavity; however, an approximately 1.02 Å-wide bottleneck was observed in this entrance tunnel. Thereafter, six amino acid residues (S412, P413, T414, T436, V437, and W438) were identified, which potentially form the bottleneck at the substrate entrance tunnel (Figure 3d). We assumed that large amino acid side chains present at the entrance tunnel forms the bottleneck and may partially block the entrance tunnel of PmLAAD, thus deterring substrate entry at the catalytic center. To verify whether these six residues are responsible for the formation of the entrance tunnel bottleneck, alanine-scanning mutagenesis was performed at the tunnel.

Alanine scanning is a common method in protein evolution engineering. Herein, we substituted the aforementioned eight candidate residues in the wild type enzyme with smaller alanine residues to enlarge the bottleneck radius of entrance tunnel and change the binding cavity for efficient substrate access and binding. The wild type PmLAAD (PmLAAD^{WT}) and eight mutants thus generated (PmLAAD^{Q92A}, PmLAAD^{M440A}, PmLAAD^{S412A}, PmLAAD^{P413A}, PmLAAD^{T414A}, PmLAAD^{T436A}, PmLAAD^{V437A}, and PmLAAD^{W438A}) were evaluated computationally via molecular dynamics (MD) simulations to analyze the substrate entrance tunnel geometry and changes in the binding cavity. Both of mutants PmLAAD^{Q92A} and PmLAAD^{M440A} displayed a significant improvement in the volume of the binding cavity compared to PmLAAD^{WT} (Figure 4). Along with reconfiguration, the bottleneck radius of the substrate entrance tunnel was significantly increased in mutants PmLAAD^{T436A} and PmLAAD^{W438A} (Figure 5a and Supplementary Table 3), but with no significant changes in the four other mutants (Supplementary Figure 2). In particular, mutant PmLAAD^{Q92A} showed the largest increase of approximately 59.0% in the volume of the binding cavity compared that of PmLAAD^{WT}. Mutant PmLAAD^{W438A} exhibited the largest increase in the bottleneck radius of nearly 0.51 Å compared with that of mutant PmLAAD^{WT}. Thus, mutants PmLAAD^{Q92A} and

FULL PAPER

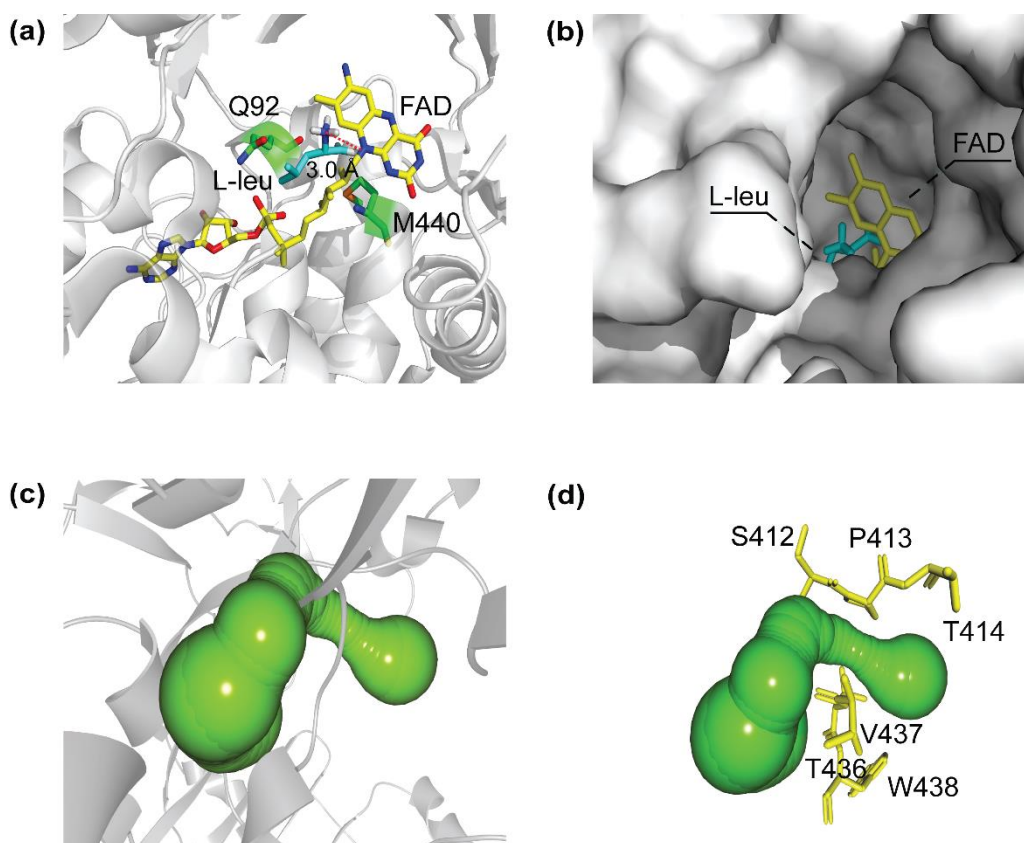


Figure 3. (a) The predicted hot spots, Q92 and M440, and highlighted as green sticks; (b) A close-up view of the PmLAAD active site in the complex with the most favorable docked position of L-leucine (cyan stick) and FAD (yellow stick); (c) The substrate entrance tunnel of PmLAAD calculated using CAVER 3.01, showed with green spheres; (d) Bottleneck residues of the substrate entrance tunnel (green spheres model) selected for mutagenesis are showed with yellow stick.

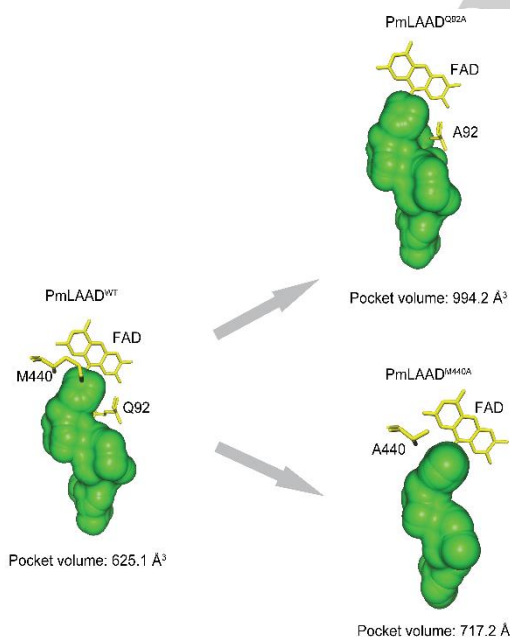


Figure 4. Comparison of the substrate binding pocket volumes of PmLAAD^{WT} and mutants PmLAAD^{Q92A} and PmLAAD^{M440A} computed using Accelrys Discovery Studio software 4.0 to determine enzyme cavities.

PmLAAD^{M440A}, while mutants PmLAAD^{T436A} and PmLAAD^{W438A} can be expected to increase the volume of the binding cavity and bottleneck radius of the entrance tunnel, respectively. Therefore, mutants PmLAAD^{Q92A}, PmLAAD^{M440A}, PmLAAD^{T436A}, PmLAAD^{W438A} were selected and expected as the optimal mutants to improve the transformation efficiency at a high substrate load by expanding the volume of the binding cavity and increasing the bottleneck radius of the entrance tunnel.

Table 1. Results of site-directed mutagenesis (alanine scanning) experiments

Enzyme	Specific activity (U mg ⁻¹ protein)	
	L-leucine	L-isoleucine
PmLAAD ^{WT}	61.73 ± 2.23	50.12 ± 1.90
PmLAAD ^{Q92A}	191.36 ± 8.32	55.34 ± 2.78
PmLAAD ^{M440A}	152.47 ± 5.34	48.27 ± 3.64
PmLAAD ^{Q92A/M440A}	58.35 ± 1.12	50.42 ± 2.67
PmLAAD ^{T436A}	65.34 ± 2.65	100.45 ± 5.56
PmLAAD ^{W438A}	67.12 ± 1.98	134.23 ± 6.12
PmLAAD ^{T436A/W438A}	70.03 ± 3.54	170.12 ± 4.43

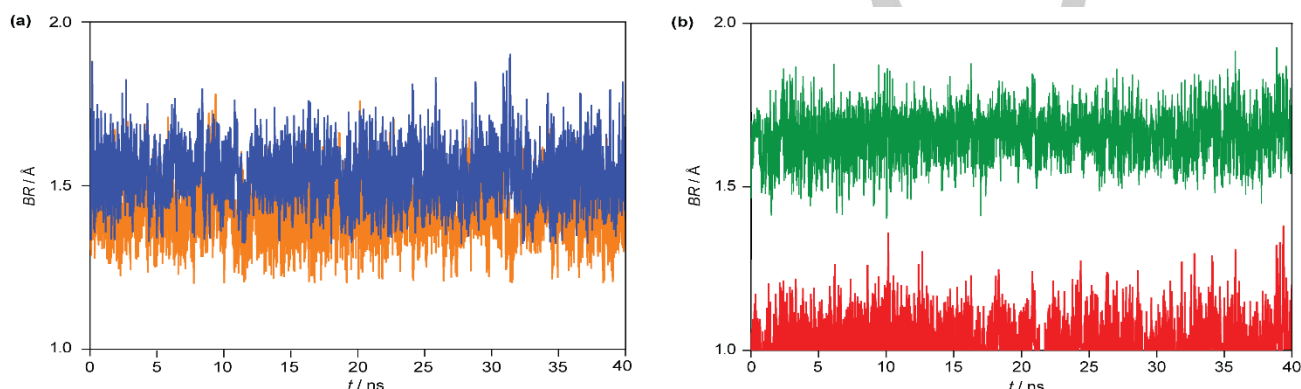
Construction and experimental evaluation of the mutants

Mutants PmLAAD^{Q92A}, PmLAAD^{M440A}, PmLAAD^{Q92A/M440A}, PmLAAD^{T436A}, PmLAAD^{W438A}, and PmLAAD^{T436A/W438A} were

FULL PAPER

Table 2. Kinetic parameters of the wild type and its mutants

Enzyme	L-leucine			L-isoleucine		
	K_m (mM)	k_{cat} (min ⁻¹)	k_{cat}/K_m (mM ⁻¹ min ⁻¹)	K_m (mM)	k_{cat} (min ⁻¹)	k_{cat}/K_m (mM ⁻¹ min ⁻¹)
PmLAAD ^{WT}	9.41 ± 0.34	3.20 ± 0.43	0.34	12.32 ± 0.12	2.46 ± 0.13	0.20
PmLAAD ^{Q92A}	4.72 ± 0.28	5.84 ± 0.48	1.23	12.02 ± 0.22	2.64 ± 0.05	0.22
PmLAAD ^{M440A}	5.12 ± 0.45	4.62 ± 0.35	0.90	12.98 ± 0.58	2.33 ± 0.41	0.21
PmLAAD ^{Q92A/M440A}	19.55 ± 1.04	4.10 ± 0.25	0.21	28.63 ± 0.82	3.15 ± 0.48	0.11
PmLAAD ^{T436A}	8.14 ± 0.12	3.01 ± 0.05	0.37	10.16 ± 0.52	3.66 ± 0.26	0.36
PmLAAD ^{W438A}	9.32 ± 0.56	3.22 ± 0.16	0.35	10.15 ± 0.28	4.88 ± 0.23	0.48
PmLAAD ^{T436A/W438A}	8.42 ± 0.43	3.50 ± 0.32	0.41	10.58 ± 0.45	7.41 ± 0.68	0.70

**Figure 5.** Time evolution of the tunnel bottleneck radius (BR) in 40 ns long MD simulations. (a) The bottleneck radius of PmLAAD^{T436A} (yellow) with 1.42 Å and PmLAAD^{W438A} (blue) with 1.53 Å; (b) The bottleneck radius increased from (1.02) Å in PmLAAD^{WT} (red) to (1.71) Å in PmLAAD^{T436A/W438A} (green). The tunnels were analyzed using CAVER 3.01

generated via site-directed mutagenesis, and their specific activities and steady-state kinetic parameters and those of PmLAAD^{WT} for L-leucine and L-isoleucine were detected and enlisted in Tables 1 and 2, respectively.

As shown in Table 1, the specific activities of mutants PmLAAD^{Q92A}, PmLAAD^{M440A}, PmLAAD^{Q92A/M440A}, PmLAAD^{T436A}, PmLAAD^{W438A}, and PmLAAD^{T436A/W438A} on L-leucine were 191.36 U mg⁻¹, 152.47 U mg⁻¹, 58.35 U mg⁻¹, 65.34 U mg⁻¹, 67.12 U mg⁻¹, and 70.03 U mg⁻¹, respectively. Among them, only the specific activities of mutants PmLAAD^{Q92A}, PmLAAD^{M440A} increased significantly in comparison with those of PmLAAD^{WT} (61.73 U mg⁻¹). Hence, the kinetic parameters of mutants PmLAAD^{Q92A} and PmLAAD^{M440A} were assessed and enlisted in Table 2. The k_{cat} and K_m values of mutant PmLAAD^{Q92A} and PmLAAD^{M440A} increased to 182.5% and 144.4%, decreased to 199.4% and 183.8%, resulting in a 361.8% and 264.7% increase in k_{cat}/K_m , respectively, compared with that of the PmLAAD^{WT}. Mutations A92 and A440 are located at the binding cavity, indicating that the increases in the volume of binding cavity may led to an increase in catalytic efficiency of enzyme to L-leucine, however, the mutations at the entrance tunnel did not significantly increase the k_{cat}/K_m .

Similarly, the specific activities of mutants PmLAAD^{Q92A}, PmLAAD^{M440A}, PmLAAD^{Q92A/M440A}, PmLAAD^{T436A}, PmLAAD^{W438A}, and PmLAAD^{T436A/W438A} to L-isoleucine were also determined. With mutations in the entrance tunnel (PmLAAD^{T436A}, PmLAAD^{W438A}, and PmLAAD^{T436A/W438A}), their specific activities

increased to 100.45 U mg⁻¹, 134.23 U mg⁻¹, and 170.12 U mg⁻¹, respectively. However, mutations in the binding pocket (PmLAAD^{Q92A}, PmLAAD^{Q92A}, and PmLAAD^{Q92A/M440A}) were unaccompanied by significant changes in the specific activity of L-isoleucine. The data for the k_{cat} and k_{cat}/K_m is summarized in Table 2. The double mutant (PmLAAD^{T436A/W438A}) showed a 3- and 3.5-fold improvement in k_{cat} and k_{cat}/K_m , respectively. These results emulate the increased entrance tunnel of PmLAAD^{T436A/W438A} with the largest bottleneck radius of 1.71 Å (Figure 5b and Supplementary Table 3). However, the double mutant (PmLAAD^{Q92A/M440A}) also exhibited a significant reduction in k_{cat}/K_m in comparison with PmLAAD^{WT}, concurrent with the results observed with L-leucine. These results indicate that the bottleneck radius of the entrance tunnel is the key limiting factor influencing the entry of L-isoleucine, rather than the broadening the binding cavity. Furthermore, expression levels of PmLAAD^{Q92A} and PmLAAD^{T436A/W438A} mutants were consistent with the PmLAAD^{WT} (Supplementary Figure 3).

We further examined the activity of PmLAAD^{Q92A} and PmLAAD^{T436A/W438A} mutants compared with that of previous substrates **5a** and **6a**. As shown in Supplementary Table 5, PmLAAD^{WT} displayed very low activity towards **5a** and **6a**. In contrast, its two mutants PmLAAD^{Q92A} and PmLAAD^{T436A/W438A} with a larger substrate-binding cavity and entrance tunnel, respectively, displaying improved activity towards bulky

FULL PAPER

Table 3. Production of α -KIC by the wild type and its mutants on 3-L scale

Substrate	Enzyme	65 (g L ⁻¹)		110 (g L ⁻¹)	
		Titer (g L ⁻¹)	Conversion (%)	Titer (g L ⁻¹)	Conversion (%)
L-leucine	PmLAAD ^{WT}	62.7	97.2	62.8	57.5
	PmLAAD ^{Q92A}	63.4	98.3	107.1	98.1
	PmLAAD ^{M440A}	63.8	98.9	93.6	85.8
	PmLAAD ^{Q92A/M440A}	45.5	70.5	42.8	39.2

Table 4. Production of α -KMV by the wild type and its mutants on 3-L scale

Substrate	Enzyme	55 (g L ⁻¹)		100 (g L ⁻¹)	
		Titer (g L ⁻¹)	Conversion (%)	Titer (g L ⁻¹)	Conversion (%)
L-isoleucine	PmLAAD ^{WT}	49.3	90.3	50	50.4
	PmLAAD ^{T436A}	54.5	99.8	74.2	74.8
	PmLAAD ^{W438A}	54.5	99.1	82.5	83.2
	PmLAAD ^{T436A/W438A}	54.4	99.7	98.9	99.7

substrates. Particularly for PmLAAD^{T436A/W438A}, wherein the enlarged entrance tunnel exhibited specific activities of 15.03 U mg⁻¹ and 12.12 U mg⁻¹ toward **5a** and **6a** compared with the PmLAAD^{WT} (10.91 U mg⁻¹ and 5.12 U mg⁻¹ for **5a** and **6a**, respectively).

Synthesis of α -KIC and α -KMV on a 3-L scale

As shown in Table 3, the α -KIC titer of mutants PmLAAD^{Q92A}, PmLAAD^{M440A}, and PmLAAD^{Q92A/M440A}, with 65 g L⁻¹ and 110 g L⁻¹ L-leucine, were compared on the 3-L scale. When 65 g L⁻¹ L-leucine was introduced in the transformation broth, α -KIC levels and conversion rate were 63.4 g L⁻¹, 63.8 g L⁻¹ and 45.5 g L⁻¹ for mutants PmLAAD^{Q92A}, PmLAAD^{M440A}, and PmLAAD^{Q92A/M440A}, respectively, and the corresponding conversion rate was 98.3%, 98.9% and 70.5%, respectively. Furthermore, the α -KIC titer of the PmLAAD^{WT}, PmLAAD^{Q92A}, PmLAAD^{M440A}, and PmLAAD^{Q92A/M440A} at 110 g L⁻¹ L-leucine were 62.8 g L⁻¹, 107.1 g L⁻¹, 93.6 g L⁻¹, and 42.8 g L⁻¹, respectively, with corresponding conversion rates of PmLAAD^{Q92A} and PmLAAD^{M440A} mutants being 40.6% and 28.3% higher than the corresponding value of the PmLAAD^{WT} (with 57.5% conversion), respectively. Furthermore, mutant PmLAAD^{Q92A} displayed a high space-time-yield (STY) of 214.2 g L⁻¹ d⁻¹.

The oxidative deamination catalyzed by the PmLAAD^{WT}, mutants PmLAAD^{T436A}, PmLAAD^{W438A}, and PmLAAD^{T436A/W438A} were investigated at a 3-L scale with 55 g L⁻¹ and 100 g L⁻¹ L-isoleucine (Table 4). With 55 g L⁻¹ L-isoleucine as the substrate, the conversion rate of mutants PmLAAD^{T436A}, PmLAAD^{W438A}, and PmLAAD^{T436A/W438A} was greater than 99%. Upon treatment with 100 g L⁻¹ L-isoleucine, the α -KMV titer, the conversion rate, STY of the PmLAAD^{WT} were 50 g L⁻¹, 50.4%, and 100 g L⁻¹ d⁻¹, respectively. For the PmLAAD^{T436A/W438A} mutant, the α -KMV titer, the conversion rate, and the STY were 98.9 g L⁻¹, 99.7%, and 197.6 g L⁻¹ d⁻¹, respectively. As expected, increased catalytic efficiencies were achieved with the most active mutants (PmLAAD^{Q92A} and PmLAAD^{T436A/W438A}) at 110 g L⁻¹ L-leucine and 100 g L⁻¹ L-isoleucine, consistent with results from MD simulations.

Discussion

In this study, PmLAAD, derived from *P. mirabilis*, exhibited

relative high activity with both L-leucine and L-isoleucine and was overexpressed in *E. coli* BL21(DE3), the catalytic efficiency was further improved through protein engineering. Upon reshaping the substrate binding cavity for L-leucine in mutant PmLAAD^{Q92A}, the titer and conversion rate of α -KIC increased to 107.1 g L⁻¹ and 98.1%, respectively. Similarly, an increase in the average bottleneck radius of the entrance tunnel in mutant PmLAAD^{T436A/W438A}, the titer, and conversion rate of α -KMV from L-isoleucine increased to 98.9 g L⁻¹ and 99.7%, respectively.

For PmLAAD, the binding sites of the isopropyl moiety of L-leucine occupied by side chain of residues Q92 was presumed as a spatial barrier preventing the binding of L-leucine, presenting severe steric clash between the backbone of L-leucine and the FAD isoalloxazine moiety (Figure 3a), leading to only 57.5% conversion of PmLAAD^{WT} with 110 g L⁻¹ L-leucine (Figure 2b and Table 3). With the PmLAAD^{Q92A} mutant, the smaller side-chain of A92 generated a larger binding cavity and increased the volume of the substrate-binding cavity of mutant PmLAAD^{Q92A} by 59.0%, with the distance between L-leucine and FAD increased from 3 Å to 3.6 Å, as shown in Supplementary Figure 4a. Consequently, the substrate bound more efficiently at the cavity with reduced steric clash between L-leucine backbone amide moiety and the FAD isoalloxazine moiety compared to the PmLAAD^{WT} enzyme. Consequently, its conformation was significantly altered, and the k_{cat}/K_m value for L-leucine was increased 3.6-fold. As shown in Supplementary Table 4, the substrate binding energy in the PmLAAD^{WT} was -3.4 kcal mol⁻¹, and that of the mutant PmLAAD^{Q92A} was -4.6 kcal mol⁻¹, consistent with the increased affinity. The residues located at the binding cavity often exhibited important effects on substrate binding^[24] because these key residues determine the volume, shape and conformational flexibility of the substrate binding cavity.^[25] Numerous studies reported that replacement of these key residues can alter the volume, geometry, and conformational flexibility of the substrate binding cavity, thereby altering the catalytic profile of the enzyme, such as substrate specificity and stereoselectivity.^[26] For instance, alcohol dehydrogenase variants engineered by replacing bulky residues constituting the active site altered the volume of the substrate binding cavity, thus accommodating a broader range of substrates.^[25] Reconfiguration of the active pocket of amine dehydrogenases by fine-tuning two hotspots at the distal end of the substrate binding cavity can significantly expand the scope for substrate binding.^[27] Similarly, conformational dynamics of the

FULL PAPER

substrate-binding site of lipase was engineered, thereby increasing the high R-enantioselectivity from 8% to 99%.^[24]

The substrate entrance tunnel also significantly affect the catalytic activity, substrate specificity, and stereoselectivity of the enzyme.^[28] In this study, threonine and tryptophan residues in the entrance tunnel were identified using MD simulations were responsible for the narrow bottleneck radius; consequently, only 50.4% conversion rate of PmLAAD^{WT} at a high L-isoleucine concentration of 100 g L⁻¹. When residues T436 and W438 were simultaneously mutated to a smaller non-polar alanine, mutant PmLAAD^{T436A/W438A} exhibited 0.69 Å increases in the bottleneck radius of the entrance tunnel. Positive mutations toward L-isoleucine were located proximal to the substrate entrance tunnel of the structure. As shown in Supplementary Figure 4b, residues T436 and W438 may constitute the entrance of the tunnel, comprising the binding site for the L-isoleucine side chain. The short distances between the L-isoleucine and T436 and W438 were 3.2 Å and 3.0 Å, respectively, resulting in steric hindrance at the narrowest section of the entrance tunnel. In addition, the indole side chain of W438 would result in steric clash with the FAD isoalloxazine moiety (Supplementary Figure 4b). Therefore, both residues played an important role in L-isoleucine entry and binding and influenced enzyme activity. As shown in Supplementary Figure 4c and Table 3, the entrance tunnel of the mutant PmLAAD^{T436A/W438A} was obviously larger than that of the PmLAAD^{WT}, and the distances between the L-isoleucine and A436 and A438 increased to 3.7 Å and 3.5 Å, respectively, allowing for substrate L-isoleucine to accept a productive conformation more easily and for increased k_{cat} , in consistent with the determined kinetic parameters. Consequently, the k_{cat}/K_m value, the titer, and the conversion rate of PmLAAD^{T436A/W438A} increased markedly, although the small side chain of alanine led to weak substrate affinity. Furthermore, binding energies of mutant PmLAAD^{T436A/W438A} and PmLAAD^{WT} were -3.4 kcal mol⁻¹ and -3.2 kcal mol⁻¹, respectively, consistent with the experimentally determined K_m values. These results indicate that engineering the substrate entrance tunnel may be an effective strategy to increase the catalytic efficiency of the enzyme.^[29] Numerous examples indicate that modifying the size or physicochemical properties of the substrate entrance tunnel can significantly increase the catalytic activity of the enzyme.^[28, 30] For example, residues F128 and M145, located in the tunnel of epoxide hydrolase *BmEH*, which reportedly restrict product release, were mutated to alanine. Two mutants, F128A and M145A, expanded the potential site of product release, displaying 42- and 25-fold greater activity than the wild type enzyme.^[31] Engineering of key residues surrounding the entrance tunnel of monoamine oxidase MAO-N decreased polarity in the entrance tunnel, which was more advantageous for the entry and release of hydrophobic substrates and products, thereby increasing the catalytic activity of the enzyme.^[28]

α -KIC and α -KMV as vital α -keto acids are extensively used in feeds and pharmaceuticals.^[1b] Studies have attempted to synthesize them through chemical synthesis,^[5] microbial fermentation,^[6] and enzymatic transformation.^[22a, 32] Among these, chemical methods not only need a multistep process but also use harsh reagents and produce toxic wastes,^[5, 33] thus deterring their

industrial production. As an alternative, *Corynebacterium glutamicum* was genetically engineered to synthesize α -KIC, yielding a titer of only 9.23 g L⁻¹.^[6] Recently, 69.1 g L⁻¹ α -KIC has been efficiently synthesized at a 50.3% conversion rate by expressing L-AAD derived from *Proteus vulgaris* in *E. coli* BL21,^[22a] followed by an attempt to optimize protein expression levels; however, α -KIC titer only increased to 86.55 g L⁻¹ within 20 h.^[22b] In addition, although the procedure for synthesizing α -KMV using amino acid oxidase has been briefly outlined, the yield is very low (less than 10 g L⁻¹).^[32] In this study, two mutants PmLAAD^{Q92A} and PmLAAD^{T436A/W438A} of PmLAAD were used to convert L-leucine and L-isoleucine to α -KIC (107.1 g L⁻¹) and α -KMV (98.9 g L⁻¹) in the 3-L scale fermenter within 12 h. Compared with the titers reported in the aforementioned studies, the production of α -KIC and α -KMV were increased in the present study. In conclusion, the present results indicate that augmentation of the substrate-binding cavity and entrance tunnel of PmLAAD can facilitate effective industrial synthesis of α -KIC and α -KMV.

Experimental Section

Materials

The expression plasmid pET-28a (+) and the host strain *E. coli* BL21 (DE3) were purchased from Novogen (Madison, WI). The restriction enzymes (*Bam*HI, *Xho*I, *Dpn*I, and *AVr*II), T4 DNA ligase, primerSTAR polymerase, plasmid miniprep kit, and agarose gel DNA purification kit were supplied by TaKaRa (Dalian, China). All other chemicals and solvents were obtained commercially.

Molecular modeling and MD simulations

The 3D structural models of PmLAAD and its mutants were constructed based on X-ray crystal structures of the L-AAD from *Proteus myxofaciens* (PDB ID: 5fjm) by homology modeling^[34]. The 3D structure of L-leucine, L-isoleucine and FAD were downloaded from the ChemSpider (<http://www.chemspider.com/>). The Dali server (<http://ekhidna2.biocenter.helsinki.fi/dali/>) was used for a protein structure similarity comparison. All structures were prepared for analysis by removing ligands and water molecules. Auto Dock Vina then was used to obtain the starting structure of the PmLAAD in complex with the substrate L-leucine.^[35] Missing atoms and hydrogen were added to the enzyme using the GROMACS 4.5.5 simulation package (<http://www.gromacs.org/>). The whole system was immersed in an explicit TIP 3P water box and extended with a thickness of at least 10 Å from the dissolved atoms in each dimension.^[36] Sodium ions were added to neutralize each system and the protonation state of residues was set according to pH 7.0. MD simulations were performed by using the GROMACS 4.5.5 and an AMBER03 force field. Initially, each system was subjected to a five-round energy minimization with the steepest descents method. Each round was relaxed for 1000 steps. After that, each the system was heated from the 0 to 300 K under an NVT ensemble by Langevin dynamics. Subsequently, an NPT ensemble was applied for the

FULL PAPER

next 1 ns, followed by 40 ns production MD in 2 fs steps for data collection. All simulations were performed individually for both the complexes of PmLAAD and its mutants. Substrate cavity volumes were calculated in Accelrys Discovery Studio 4.1 by searching for cavities with no substrate bound. The MD trajectories were further analyzed to identify relevant substrate binding poses, and substrate entrance structures that were sampled and calculated in the simulation using CAVER 3.01. The Min. probe radius was 0.9 Å and shell depth was 4 Å. The initial starting points for calculation were defined by active site residues. All images of the structures shown here were generated using PyMol and CAVER.

Mutants construction

The primers used for gene cloning and PmLAAD plasmid construction are summarized in Supplementary Table 6. PmLAAD encoding gene *aad* (GenBank accession number U35383) from *P. mirabilis* was inserted into the pET-28a (+) using the restriction sites *Bam*HI and *Xho*I for expression in *E.coli* BL21 (DE3). Site-directed mutagenesis was carried by PCR using mutagenic primers (listed in Supplementary Table 4) and plasmid pET-28a (+)-PmLAAD as template. *Dpn*I (1 µL of 10 U µL⁻¹) was added to 25 µL of the PCR reaction mixture and incubated for 3 h at 37 °C to eliminate the template plasmid. The digested product was transformed into *Escherichia coli* JM109 cells for amplification and DNA sequencing until all designed mutants were obtained. Subsequently, plasmid pET-28a mutants were extracted and transformed into *E.coli* BL21 (DE3) for target protein expression.

Analytical methods

The optical density at 600 nm (OD₆₀₀) was measured using a spectrophotometer. The α-keto acids concentrations were measured by HPLC (Agilent 1100 series, Santa Clara, CA, USA) using a VWD detector. Samples were separated on an Aminex HPX-87H (7.8 × 300 mm, Bio-Rad Laboratories Inc., Hercules, CA, USA) column eluted with 0.005 mol L⁻¹ H₂SO₄ at a constant flow rate of 0.6 mL min⁻¹ (35 °C) and detected by monitoring absorbance at 210 nm. The mobile phase was filtered through a 0.22-µm membrane and ultrasonically degassed before use. Samples were centrifuged at 12,000 × g for 5 min and then the supernatants were filtered using 0.22-µm filter membrane.

Protein expression and purification

E.coli BL21 (DE3) cells carrying the recombinant plasmid were cultivated in 2 mL of LB medium containing Kanamycin (100 µg mL⁻¹) at 37 °C and 200 rpm for 12 h. The overnight culture was inoculated into 100 mL LB medium and grown at 37 °C and 200 rpm in a rotary shaker. When the optical density (OD₆₀₀) of culture reached 0.6-0.8, 0.4 mM IPTG was added to induce the enzyme expression at 25 °C for an additional 12 h. The cells were harvested by centrifugation at 6,000 × g for 5 min at 4 °C and resuspended in Tris-HCl buffer (50 mM, pH 8.0). The cells were lysed by ultrasonication in an ice bath, and the supernatant was

collected by centrifugation at 14,000 × g for 1 h at 4 °C. The crude enzyme solution was used in subsequent analyses.

Activity assay

To measure the enzyme activities of wild type PmLAAD and its mutants, the reaction mixture containing 30 mM L-amino acids and a certain enzyme was incubated with 50 mM Tris-HCl buffer (pH 8.0) in a final volume of 2 mL at 30 °C for 15 min. The reaction was stopped with centrifugation at 12,000 × g for 5 min, samples were analyzed by HPLC. One unit of enzyme is defined as the amount of enzyme producing 1 µmol of α-keto acids per minute. The protein concentration was determined by the Bradford protocol,^[37] with bovine serum albumin as the standard. All experiments were conducted in triplicate.

Determination of kinetic parameters

The kinetic parameters were determined by measuring the initial rate of enzymatic reaction at different concentrations of substrate (2-100 mM) in Tris-HCl buffer (50 mM, pH 8.0) at 30 °C. The samples were withdrawn, extracted, and analyzed by HPLC, and *K_m* and *k_{cat}* then calculated by nonlinear regression according to the Michaelis-Menten equation using Origin software. All experiments were performed in triplicate.

Fed-batch fermentation

Seed cultures were grown overnight in 50 mL of LB medium and then sub-cultured in 150 mL of LB medium at 37°C for 10 h. Cells were harvested to inoculate 3 L of TB medium (24 g L⁻¹ yeast extract, 12 g L⁻¹ peptone, 4 g L⁻¹ glycerol, 2.31 g L⁻¹ KH₂PO₄, 16.42 g L⁻¹ K₂HPO₄·3H₂O) for fed-batch fermentation in a 7.5-L INFORS fermenter. The temperature, pH, agitation rate, and aeration rate were adjusted to 37 °C, 7.0, 600 rpm, and 1.0 vvm, respectively. Induction of enzyme expression was performed when the culture reached an OD₆₀₀ of 3-5, by adding optimized lactose and changing the cultivation temperature to 30 °C. When the dissolved oxygen (DO) level increased rapidly (demonstrating glycerol in the medium was completely exhausted), the system was supplied with 100 g L⁻¹ yeast extract, 25 g L⁻¹ peptone, and 400 g L⁻¹ glycerol at a rate of 16 mL h⁻¹. The strain was harvested as a whole cell catalyst by centrifugation at 6,000 × g for 8 minutes.

Biocatalytic oxidative deamination reaction on analytical scale

A 1-mL scale biocatalytic reaction mixture containing lyophilized whole cell catalyst PmLAAD (4 mg), substrate (50 mM), and Tris-HCl buffer (50 mM, pH 8.0) was incubated at 30 °C and 200 rpm for 24 h. Then the reaction mixture was stopped with centrifugation at 12,000 × g for 5 min. The conversion rate was measured by HPLC. 20-mL scale biocatalytic reactions were also conducted to optimize transformation reactions of PmLAAD with L-leucine and L-isoleucine as the substrates. A 20 mL reaction mixture contained wet whole cell catalysts PmLAAD (0.1-0.6 g),

FULL PAPER

L-leucine (1.3-2.2 g) or L-isoleucine (0.3-1.5 g), and Tris-HCl buffer (50 mM, pH 8.0) was incubated at 30°C and 200 rpm for 20 h. 500 μ L of sample was taken timely after vigorous shaking, centrifuged at 12,000 \times g for 5 min before analysis by HPLC.

Production of α -KIC and α -KMV on a 3-L scale

For large scale production of α -KIC and α -KMV, L-leucine (65, 110 g L⁻¹) or L-isoleucine (55, 100 g L⁻¹) was dissolved in a 3 L Tris-HCl buffer (50 mM, pH 8.0). Wet whole cell catalysts PmLAAD mutants (20 g L⁻¹) were added to initiate the reaction. The pH was automatically maintained at 8.0 by titrating with 4 M NaOH. The reaction mixture in a 7.5-L INFORS fermenter was stirred at 30 °C and 500 rpm. The concentrations of α -KIC and α -KMV were determined using the HPLC method as described above.

Acknowledgements

This work was financially supported by the National First-class Discipline Program of Light Industry Technology and Engineering (LITE2018-08), the Key Technologies R & D Program of Jiangsu Province (BE2018623), and the Scientific and Technological Innovation Leading Talents of National "Ten Thousand Talent Program" (2018).

Keywords: catalytic efficiency • L-amino acid deaminase • protein engineering • α -ketoisocaproate • α -keto- β -methylvalerate

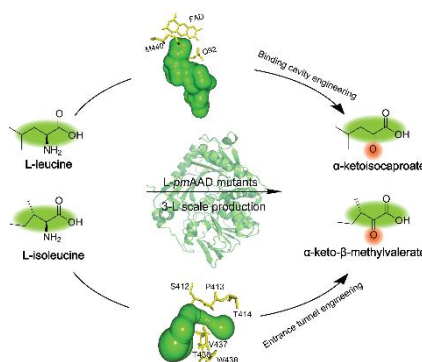
- [1] a) S. Atsumi, T. Hanai, J. C. Liao, *Nature*. **2008**, *451*, 86-89; b) Y. Song, J. H. Li, H. D. Shin, L. Liu, G. C. Du, J. Chen, *Bioresource Technol.* **2016**, *219*, 716-724.
- [2] A. Schouteeten, Y. Christidis, **1985**, European patent 0132201.
- [3] K. C. Kyowa Hakko, **1984**, Japanese patent 59199652.
- [4] S. Alain, C. Yani, **1985**, US patent 4518800.
- [5] A. J. Cooper, J. Z. Ginos, A. Meister, *Chem. Rev.* **1983**, *83*, 321-358.
- [6] V. Buckle-Vallant, F. S. Krause, S. Messerschmidt, B. J. Eikmanns, *Appl. Microbiol. Biotechnol.* **2014**, *98*, 297-311.
- [7] H. B. Coban, A. Demirci, P. H. Patterson, R. J. Elias, *Bioproc Biosyst Eng.* **2014**, *37*, 2343-2352.
- [8] L. Pollegioni, P. Motta, G. Molla, *Appl. Microbiol. Biotechnol.* **2013**, *97*, 9323-9341.
- [9] G. Molla, R. Melis, L. Pollegioni, *Biotechnol. Adv.* **2017**, *35*, 657-668.
- [10] Y. P. Xue, C. H. Cao, Y. G. Zheng, *Chem. Soc. Rev.* **2018**, *47*, 1516-1561.
- [11] M. Yoshimoto, M. Okamoto, K. Ujihashi, T. Okita, *Langmuir*. **2014**, *30*, 6180-6186.
- [12] M. García-García, I. Martínez-Martínez, A. Sánchez-Ferrer, F. García-Carmona, *Biotechnol. Prog.* **2008**, *24*, 187-191.
- [13] a) P. Ödman, W. B. Wellborn, A. S. Bommaribus, *Tetrahedron: Asymmetry*. **2004**, *15*, 2933-2937; b) W. Greschner, C. Lanzerath, T. Reß, K. Tenbrink, S. Borchert, A. Mix, W. Hummel, H. Gröger, *J. Mol. Catal. B-Enzym.* **2014**, *103*, 10-15.
- [14] A. L. Ahmad, E. M. Low, S. R. Abd Shukur, *J. Mol. Catal. B-Enzym.* **2013**, *88*, 26-31.
- [15] N. M. W. Brunhuber, J. B. Thoden, J. S. Blanchard, J. L. Vanhooke, *J. Biochem.* **2000**, *39*, 9174-9187.
- [16] T. Li, A. B. Kootstra, I. G. Fotheringham, *Org. Process Res. Dev.* **2002**, *6*, 533-538.
- [17] Y. Ju, S. Tong, Y. Gao, W. Zhao, Q. Liu, Q. Gu, J. Xu, L. Niu, M. Teng, H. Zhou, *J. Struct. Biol.* **2016**, *195*, 306-315.
- [18] Y. Hou, G. S. Hossain, J. Li, H. D. Shin, G. Du, L. Liu, *Appl. Microbiol. Biotechnol.* **2016**, *100*, 2183-2191.
- [19] R. X. Li, H. G. Sakir, J. Li, H. D. Shin, G. Du, J. Chen, L. Liu, *RSC Adv.* **2017**, *7*, 6615-6621.
- [20] G. S. Hossain, J. Li, H. D. Shin, L. Liu, M. Wang, G. Du, J. Chen, *J. Biotechnol.* **2014**, *187*, 71-77.
- [21] G. S. Hossain, J. Li, H. D. Shin, G. Du, M. Wang, L. Liu, J. Chen, *PLoS One*. **2014**, *9*, e114291.
- [22] a) Y. Song, J. Li, H. D. Shin, G. Du, L. Liu, J. Chen, *Sci. Rep.* **2015**, *5*, 12641; b) Y. Song, J. Li, H. D. Shin, L. Liu, G. Du, J. Chen, *PLoS One*. **2017**, *12*, e0179229.
- [23] L. Liu, G. S. Hossain, H. D. Shin, J. Li, G. Du, J. Chen, *J. Biotechnol.* **2013**, *164*, 97-104.
- [24] B. Yang, H. Wang, W. Song, X. Chen, J. Liu, Q. Luo, L. Liu, *ACS Catal.* **2017**, *7*, 7593-7599.
- [25] Y. Nie, S. Wang, Y. Xu, S. Luo, Y. L. Zhao, R. Xiao, G. T. Montelione, J. F. Hunt, T. Szyperski, *ACS Catal.* **2018**, *8*, 5145-5152.
- [26] S. Jemli, D. Ayadi-Zouari, H. B. Hlima, S. Bejar, *Crit. Rev. Biotechnol.* **2016**, *36*, 246-258.
- [27] F. F. Chen, G. W. Zheng, L. Liu, H. Li, Q. Chen, F. L. Li, C. X. Li, J. H. Xu, *ACS Catal.* **2018**, *8*, 2622-2628.
- [28] G. Y. Li, P. Y. Yao, R. Gong, J. L. Li, P. Liu, R. Lonsdale, Q. Q. Wu, J. P. Lin, D. M. Zhu, M. T. Reetz, *Chem. Sci.* **2017**, *8*, 4093-4099.
- [29] L. J. Kingsley, M. A. Lill, *Proteins*. **2015**, *83*, 599-611.
- [30] Z. J. Luan, F. L. Li, S. Dou, Q. Chen, X. D. Kong, J. Zhou, H. L. Yu, J. H. Xu, *Catal. Sci. Technol.* **2015**, *5*, 2622-2629.
- [31] X. D. Kong, S. Yuan, L. Li, S. Chen, J. H. Xu, J. Zhou, *Proc. Natl. Acad. Sci. U. S. A.* **2014**, *111*, 15717-15722.
- [32] A. Meister, *Methods Enzymol.* **1957**, *3*, 404-414.
- [33] D. Balducci, P. A. Conway, G. Sapuppo, H. Müller-Bunz, F. Paradisi, *Tetrahedron*. **2012**, *68*, 7374-7379.
- [34] A. Waterhouse, M. Bertoni, S. Bienert, G. Studer, G. Tauriello, R. Gumieny, F. T. Heer, T. A. P. de Beer, C. Rempfer, L. Bordoli, R. Lepore, T. Schwede, *Nucleic Acids Res.* **2018**, *46*, W296-W303.
- [35] O. Trott, A. J. Olson, *J. Comput. Chem.* **2010**, *31*, 455-461.
- [36] W. L. Jorgensen, J. Chandrasekhar, J. D. Madura, R. W. Impey, M. L. Klein, *J. Chem. Phys.* **1983**, *79*, 926-935.
- [37] N. J. Kruger, *The Bradford method for protein quantitation*, Humana Press, New Jersey, **2002**.

FULL PAPER

Entry for the Table of Contents

FULL PAPER

In this study, we developed an efficient enzymatic strategy for industrial production of α -KIC and α -KMV from L-leucine and L-isoleucine, respectively, employing enzyme PmLAAD. Poor productivity in this process due to the insufficient catalytic efficiency of PmLAAD. In an effort to increase the catalytic efficiency of wild type PmLAAD for the improvement of α -KIC and α -KMV production, we engineered the PmLAAD substrate binding cavity and entrance tunnel.



Yuxiang Yuan, Wei Song, Jia Liu,
Xiulai Chen, Qiuling Luo, and
Liming Liu*

Page No. – Page No.

Production of α -ketoisocaproate
and α -keto- β -methylvalerate by
engineered L-amino acid
deaminase